Room-Temperature Si Etching in NO/F2 Gases and the Investigation of Surface Reaction Mechanisms

Article *in* The Journal of Physical Chemistry C · February 2013

Impact Factor: 4.77 · DOI: 10.1021/jp3119132

5 authors, including:

Satomi Tajima
Toyota Central R & D Labs., Inc.
28 PUBLICATIONS **153** CITATIONS
SEE PROFILE

Toshio Hayashi
Nagoya University
70 PUBLICATIONS **503** CITATIONS
SEE PROFILE

Kenji Ishikawa
Nagoya University
166 PUBLICATIONS **763** CITATIONS
SEE PROFILE

Makoto Sekine
Nagoya University
209 PUBLICATIONS **1,210** CITATIONS
SEE PROFILE

THE JOURNAL OF PHYSICAL CHEMISTRY C

Article

pubs.acs.org/JPCC

Room-Temperature Si Etching in NO/F_2 Gases and the Investigation of Surface Reaction Mechanisms

Satomi Tajima,* Toshio Hayashi, Kenji Ishikawa, Makoto Sekine, and Masaru Hori

Plasma Nanotechnology Research Center (PLANT), Graduate School of Engineering, Nagoya University, Furo-cho, Chikusa-ku, Nagoya, Aichi, Japan 464-8603

ABSTRACT: We have been investigating a plasmaless Si chemical dry etching in NO/F_2 gas mixtures using the F produced by the exothermic reaction of $F_2 + NO \rightarrow FNO + F$ at room temperature. The effect of the change in the flow rate ratio of NO and F_2, f_{NO}/f_{F_2}, on the etch rate, the chemical bonding structures, and the surface morphology was measured by laser microscopy, Fourier transform infrared spectrometer, scanning electron microscopy, and scanning white light interferometry and results were compared with the calculated F flux. Total energy variations and their changes in chemical bonding structures before and after the reactions of molecules in the gas phase and the Si surface were considered using the molecular orbital (MO) method. On the basis of the MO calculation using a Si(100)-2×1 cluster model, F was necessary to form a dangling bond at the surface of Si that would trigger subsequent chemical reactions of Si with F_2, NO, F, or FNO. The etch rate and surface roughness increased with the addition of NO up to the f_{NO}/f_{F_2} = 1.0 to 1.5 and then decreased due to the reduction of F flux in the gas phase together with the presence of the Si-NO and the Si-FNO bonds that would block the interaction of Si with F_2 and F.

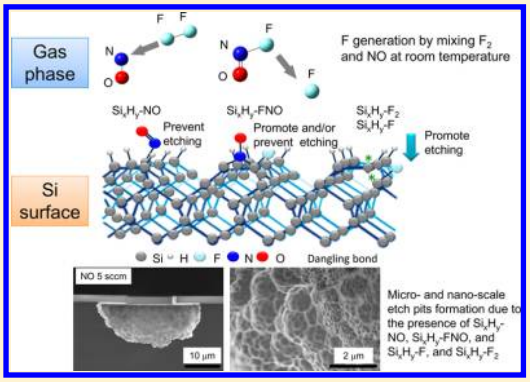

1. INTRODUCTION

A new Si dry-etching concept that is safe, low-cost, and low-energy-consuming is necessary to fabricate surface texturing of solar cells[1] through silicon via (TSV) integration architecture for multilayered packaging,[2] removal of sacrificial layer of microelectromechanical system (MEMS),[3] and cleaning of the chamber wall of chemical vapor deposition (CVD).[4] The isotropic Si etching[5] is normally performed either by the wet etching,[6] by the chemical dry etching that produces atomic fluorine (F),[7−9] or by the plasma dry etching that produces F and F ions.[10] F reactions on the Si surface have been intensively studied since the 1980s, and various reaction models have been proposed.[11−20] Wet etching techniques require expensive harsh chemical disposals. Chemical dry etching techniques use expensive or highly reactive gases such as XeF_2, BrF_3, BrF_5, ClF_3,[1,7] and plasma dry etching techniques must use the expensive power supply and the high vacuum equipment to generate plasmas.[10]

To improve the safety, reduce the process cost, and eliminate the harsh chemical disposal for the environment, the chemical dry-etching process utilizing F in the NO/F_2 gas mixture has been proposed. The mixture of F_2 and NO gases produces F by the reaction of $F_2 + NO \rightarrow FNO + F$ at room temperature. Detail investigations of F_2 and NO reaction and the determination of rate coefficient calculation were performed in the 1950−1970s,[21−25] and the results indicated that the addition of NO plays an important role in controlling F density. Hoell et al. reported that the density of F almost linearly increased with NO/F_2 molar fractions at 0 to 0.20.[23]

Lee et al. reported that mixing NO with F_2[26−28] or NF_3[29,30] downstream plasmas produced F radicals, resulting in etching of Si at the rate of 22−24 μm/min. Recently, the NO and F_2 mixture was proven to clean the SiN_x deposit in the thin-film process chamber wall without using plasmas.[31−33] However, the effectiveness of plasmaless Si chemical dry etching in NO/F_2 gases has not yet been reported.

In this study, we performed the plasmaless Si chemical dry etching using NO/F_2 gas mixtures. First, we calculated the excess energy of FNO and F produced by the reaction of NO and F_2 gases. Changes in chemical-bonding structures and total energies of Si before and after the reaction with F_2, NO, F, and FNO were calculated by the molecular orbital (MO) method to estimate the possible surface reaction pathway during chemical dry etching. Then, we varied the flow rate ratio of NO/F_2 at a room temperature and elucidated the contribution of F_2, NO, F, and FNO to the Si etching by measuring the etch rate, surface chemical bonding structures, and surface morphology while comparing the calculated F flux. On the basis of MO calculation results and experimental results, we were able to optimize the Si etch rate and surface morphology for desired applications such as the solar cell surface texturing, the through hole etching of TSV, and the sacrificial layer removal of MEMS.

Received: December 4, 2012
Revised: February 18, 2013
Published: February 25, 2013

   dx.doi.org/10.1021/jp3119132 | J. Phys. Chem. C 2013, 117, 5118−5125

2. THEORETICAL CALCULATION

The chemical reaction pathway between F_2 and NO in the gas phase was first calculated using B3LYP/6-31G+(d) in the Gaussian program[34] to estimate the change in total energy before and after the reaction. Then, the change in chemical bonding structure and total energies of Si before and after the reaction with F_2, NO, F, and FNO were calculated using B3LYP/6-31G+(d,p). The Si(100)-2×1 cluster model was employed to describe the top four layers of the Si surface. We assumed two initial surface conditions: one is two Si−H bonds at the surface (Si_9H_{14}), simulating Si−H terminated surface after HF cleaning, and the other is one Si−H bond and one Si dangling bond at the surface (Si_9H_{13}), simulating activated surface. Changes in total energies of F_2, NO, F, and FNO and Si (Si_9H_{13} and Si_9H_{14}) were plotted while varying the distance between Si and F_2, NO, F or FNO from 3.0 to 1.1 Å by every 0.02 to 0.1 Å.

3. EXPERIMENTAL SECTION

p-Type Si (100) covered by 1 μm thick SiO_2 mask with 15 μm × 15 μm square patterns and nondoped Si (100) without patterns were prepared, and they were diced into 5 mm × 15 mm samples. The patterned Si samples were used for the etch rate measurement, whereas precleaned nondoped Si samples were used for chemical analysis and surface morphology measurement. Nondoped Si samples were cleaned with acetone, ethanol, deionized (DI) water, 13% hydrochloric acid, and 49% hydrofluoric (HF) acid for 5 min, followed by rinsing the wafer with DI water for <5 s to terminate the Si surface with H.

Samples were introduced in the Pyrex tube with the inner diameter of 25 mm and the length of 150 mm and placed on top of the alumina plate, which was covered by the aluminum foil, as shown in Figure 1. The temperature of the top surface of

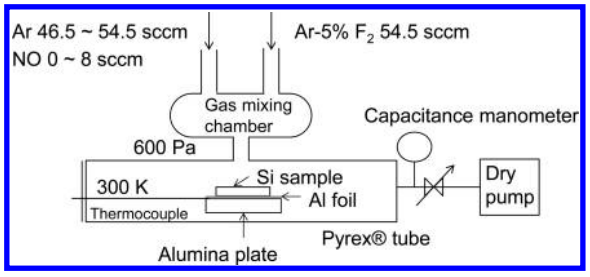

Figure 1. Experimental apparatus for the plasmaless Si chemical dry etching.

the alumina plate was measured by the K-type thermocouple. The Si sample was exposed to the gas mixture of NO at flow rate, f_{NO}, of 0 to 8 sccm (0 to 1.4×10^{-2} Pa-m^3/s) diluted with the Ar at a flow rate, f_{Ar}, of 46.5 to 54.5 sccm ($(7.9 \text{ to } 9.2) \times 10^{-2}$ Pa-m^3/s), and the Ar/5%-F_2 at a flow rate, $f_{Ar\text{-}5\%F_2}$, of 54.5 sccm (9.2×10^{-2} Pa-m^3/s), corresponding to a F_2 flow rate, f_{F_2}, of 2.7 sccm (4.6×10^{-3} Pa-m^3/s) at a room temperature of T = 300 K. The flow rate ratio of NO and F_2, f_{NO}/f_{F_2}, changed from 0 to 3. The pressure in the Pyrex tube was maintained at 600 Pa throughout the process time, t, of 5 min for Si etching with the SiO_2 mask and 0.5 min for the nondoped Si etching.

The Si etch rate was calculated from the etched depth at the middle of the 15 μm × 15 μm pattern measured by laser microscopy (VK-9700, Keyence, Osaka, Japan) divided by the etching process time of 5 min. Surface chemical bonding structures were analyzed by transmission Fourier transform infrared (FT-IR) spectroscopy (Nicolet 8700, Thermo Fisher Scientific, Waltham, MA) with the scan number of 128 and the resolution of 4 cm^{-1}. The etched sidewall and the bottom morphology were observed by scanning electron microscopy (SEM) (S-5200 Hitachi High-Technologies, Tokyo) with an acceleration voltage of 2 kV and the magnification of (1−20) × 10^3, and root-mean-square (rms) roughness measured from the 10 μm line profile in the 10 μm × 10 μm image captured by scanning white light interferometry (SWLI) with a 50× objective lens (Zygo, New View 6200, Zygo, Middlefield, CT). The etch rate and surface morphology were measured nine times from multiple samples.

4. RESULTS AND DISCUSSION

4.1. Prediction of F_2 and NO Gas-Phase Reaction. Figure 2 shows the difference in total energies and geometries

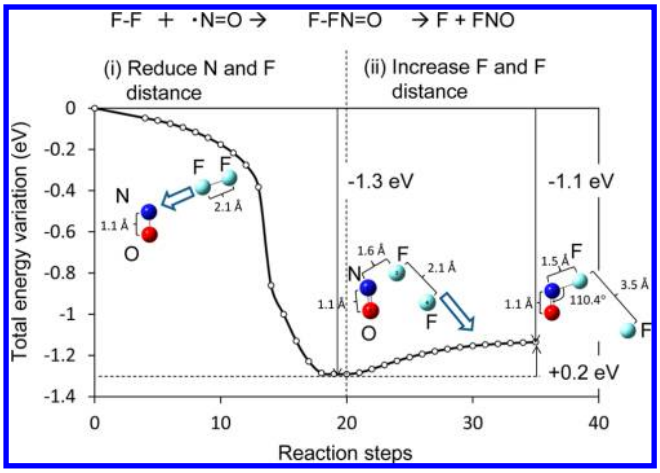

Figure 2. Relationship between the total energy variation during the reaction of F_2 + NO → F-FNO →FNO + F and the reaction step calculated by B3LYP/6-31+G(d) in Gaussian 03.

of F_2 + NO and FNO + F calculated by B3LYP/6-31 G + (d) in Gaussian 03. The calculation is based on the following procedures. First, the distance between N of NO and F of F_2 was set to 3.0 Å, indicating that F_2 and NO were not chemically reacted. Then, the distance between F and N reduced by every 0.1 Å until the potential energy became minimum to form the intermediate product of F-FNO. F-FNO was produced from the NO/F_2 gas mixture exothermically, and the difference in total energies of F_2 + NO and F-FNO was −1.3 eV. Next, the one of the F of F-FNO shown in Figure 2 was separated from FNO to produce FNO + F. The distance between F and F was changed from 2.1 to 3.5 Å in every 0.1 Å. Although the total energy of FNO + F was 0.2 eV higher than that of F-FNO, this endothermic reaction can be proceeded by the help of energy released (−1.3 eV) from the exothermic reaction of F_2 + NO → F-FNO. The difference in total energies of F_2 + NO and FNO + F was −1.1 eV. This excess energy released (1.1 eV) was distributed to F (0.8 eV) and FNO (0.3 eV) based on the inverse of mass fraction.

4.2. Prediction of the Reaction of F_2, NO, F, and FNO with Si. *(i) F_2, NO, F, and FNO Reaction with Si_9H_{14}.* We first evaluated the reaction of F_2, NO, F, and FNO with H-terminated Si surfaces using the Si(100)-2×1 cluster model (Si_9H_{14}), which simulates the nondoped Si (100) sample

dx.doi.org/10.1021/jp3119132 | J. Phys. Chem. C 2013, 117, 5118−5125

cleaned with HF and terminated with Si−H bonds in this experiment. The distance between the Si atom located at the top of the surface and the gas atoms and molecules (F_2, NO, F, and FNO) was reduced from 3.0 Å in every 0.1 Å, and the change in total energies was plotted with respect to the each reaction steps. We found that activation energies of 1.5 to 3.0 eV were necessary for the reaction of F_2, NO, and FNO with Si_9H_{14}. Therefore, these reactions would not happen in our process chamber at a room temperature. Experimental results confirmed this calculation that no etching was actually observed when Si was exposed to NO or F_2 gas alone at the room temperature.

The Si_9H_{14} could only react with F with the activation energy of 0.3 eV, as shown in Figure 3a. In the chamber that was

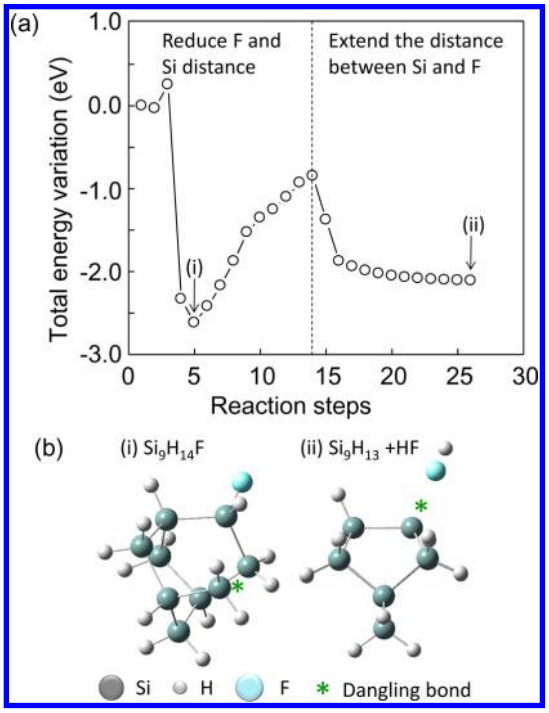

Figure 3. Change in the total energy during the reaction of F with the Si(100)-2×1 cluster model (Si_9H_{14}) calculated by B3LYP/6-31+G-(d,p) in Gaussian 09. The distance between Si and F decreased from 3.0 to 1.1 Å by every 0.1 Å. (a) The total energy variation versus the reaction steps when F approached to Si. (b) A dangling bond (marked by the arrow) could be initiated at the second layer at the fifth reaction step (i) and at the first layer at the 26th reaction step (ii).

maintained at 600 Pa, we consider that most of the total energy of F produced by F_2 + NO → F + FNO at 0.8 eV calculated in Section 4.1 was lost due to the collision with atoms and molecules present in the gas phase such as Ar, F, NO, F_2, and FNO before reaching the Si surface. However, the small fraction of F has enough total energy to overcome the activation energy of 0.3 eV to initiate the reaction between H-terminated Si and F to form a dangling bond at the Si surface (Si_9H_{14} + F → Si_9H_{13} + HF). Once the dangling bond is formed, the Si_9H_{13} + F → $Si_9H_{13}F$ reaction proceeds even at the room temperature. Experimental results confirmed that the presence of F by mixing NO- and F_2-initiated Si etching on the H-terminated Si surface, which indicated the presence of F with the total energy sufficient to overcome the activation energy of H-terminated Si, followed by the F reaction on the Si surface with the dangling bond. After the Si_9H_{14} reacted with F, two different structures with one dangling bond could be formed, as shown in Figure 3b. One was $Si_9H_{14}F$ that had the dangling bond at the second layer of Si (100), denoted as (i) in Figure 3a, and the other was Si_9H_{13} with the dangling bond at the first layer of Si (100) (Si_9H_{13}) and released the HF. The exothermic energy of −2.0 eV was released from the reaction of Si_9H_{14} + F → Si_9H_{13} + HF (denoted as Figure 3b(ii)). Because the Si(100) - 2 × 1 cluster model uses the Si−H bond instead of the Si−Si bond at the second through fourth layers, the $Si_9H_{14}F$ shown in Figure 3b(i) might not represent the actual chemical bonding structure. Therefore, we would consider reactions of Si_9H_{13} shown in Figure 3b(ii) with F_2, NO, F, and FNO in the next section.

(ii) F_2, NO, F, and FNO Reactions with Si_9H_{13}. In this section, reactions of Si_9H_{13} with F_2, NO, F, and FNO will be discussed. The Si_9H_{13} with one dangling bond, as shown in Figure 3b(ii), would react with F_2, NO, F, and FNO exothermically. The change in the total energy before and after the reaction of Si_9H_{13} + F_2, Si_9H_{13} + NO, Si_9H_{13} + F, and Si_9H_{13} + FNO was −3.5, −1.1, −3.8, and −4.1 eV, respectively. When F_2 approached the dangling bond at the Si surface, two Si−F bonds were formed at the first and second layer and one dangling bond was initiated at the first layer, as shown in Figure 4a. When NO and F approached the dangling bond at the Si

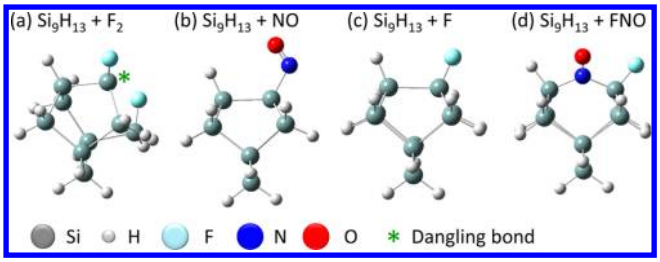

Figure 4. Change in the surface chemical structure of the Si(100)-2×1 cluster model with one dangling bond (Si_9H_{13}) after the reaction with F_2, NO, F, and FNO present in the process chamber was calculated by B3LYP/6-31+G(d,p) in Gaussian 09. The chemical structures of (a) Si_9H_{13} +F_2, (b) Si_9H_{13} + NO, (c) Si_9H_{13} + F, and (d) Si_9H_{13} + FNO that had minimum total energies.

surface, $Si_9H_{13}NO$ and $Si_9H_{13}F$ were formed, respectively, as shown in Figures 4b and 4c. When FNO approached the dangling bond at the first layer of Si_9H_{13}, several different chemical structures of $Si_9H_{13}FNO$ were formed before reaching the chemical bonding structure that had minimum total energy, as shown in Figure 4d.

The relationship between the reaction steps and the change in the total energy with the corresponding chemical bonding structures of $Si_9H_{13}FNO$ are shown in Figure 5. The distance between the Si dangling bond and N in FNO was changed from 3.0 Å in every 0.02 Å. 49 reaction steps were necessary to form $Si_9H_{13}FNO$ with the minimum total energy, as shown in Figure 5a. First, the FNO attached the Si dangling bond (reaction steps n = 1∼12) and the total energy was reduced −2.8 eV (reaction step = 13). Then, the NO rotated with respect to the Si−F bond and moved to the middle position of the Si−Si bond at the first layer (reaction steps n = 13∼46). The Si−Si bond at the first atomic layer was separated, and one or two dangling bonds were formed (reaction step n = 39 for two dangling bonds, n = 46 for one dangling bond). The NO was then incorporated at the backbone of the Si−Si bond to form

dx.doi.org/10.1021/jp3119132 | J. Phys. Chem. C 2013, 117, 5118−5125

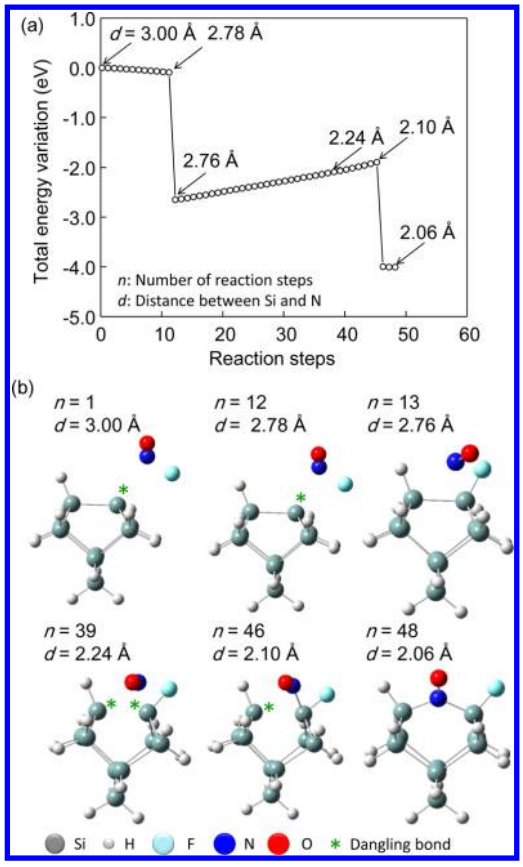

Figure 5. Change in the total energy during the reaction of the FNO approaching the surface of Si(100)-2×1 cluster model with a dangling (Si_9H_{13}) bond was calculated by B3LYP/6-31+G(d,p) in Gaussian 09. The distance between Si with the dangling bond and FNO was decreased from 3.00 to 2.06 Å by every 0.02 Å. (a) Total energy variation versus the reaction step when F approached the dangling bond. (b) Change in chemical bonding structures during the reaction of Si_9H_{13} + FNO → Si_9H_{13}FNO (reaction steps at 1, 12, 13, 39, 46, and 48).

the Si−NO−Si−F bond shown in Figure 5b (reaction steps n = 47∼49).

MO calculations indicated that F_2, NO, F, and FNO contributed to the change in surface chemical bonding structures of Si once the dangling bond was formed by the reaction of F with H-terminated Si. In the next two sections, we empirically evaluated how F influenced the change in the Si etch rate with the different f_{NO}/f_{F_2} and considered the validity of MO calculation results.

4.3. Change in Etch Rate with the Addition of NO. The etched depth at the center of the 15 μm × 15 μm pattern of the p-type Si (100) sample exposed in the NO/F_2 gas mixture for t = 5 min was measured by laser microscopy while varying the f_{NO}/f_{F_2} from 0.0 to 3.0. The etch rate was calculated from the etched depth divided by t = 5 min, and results are shown in Figure 6. The etch rate linearly increased to ∼5 μm/min with the f_{NO}/f_{F_2} up to ∼1.0. The etch rate then decreased gradually at 1.0 < f_{NO}/f_F < 2.0, followed by the significant reduction at 2.0 < f_{NO}/f_F.

To understand the cause of the change in the etch rate with respect to the f_{NO}/f_F, we estimated the F flux responsible for the etching. First, the density of F in the chamber was calculated based on the following two chemical reactions where

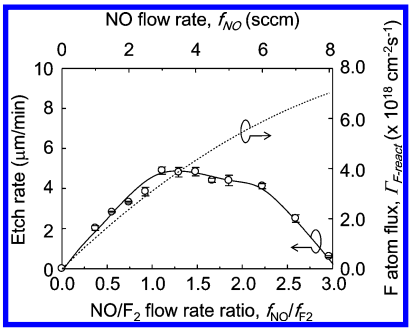

Figure 6. Relationship between the etch rate and the flow rate ratio, f_{NO}/f_{F_2}. $f_{Ar\text{-}5\%F_2}$ = 54.5 sccm (corresponding f_{F_2} = 2.7 sccm) remained constant while varying f_{NO} from 0.0 to 8.0 sccm and f_{Ar} from 46.5 to 54.5 sccm. The pressure of the chamber was maintained at 600 Pa throughout the process time of 5 min. 10% of F atom flux approaching the Si surface, $\Gamma_{F\text{-react}}$, was calculated and shown in the dotted line.

the reaction 1 is the generation of F and the reaction 2 is the loss of F.

$$F_2 + NO \xrightarrow{k_1} F + FNO \quad (1)$$

$$F + NO \xrightarrow{k_2} FNO \quad (2)$$

According to Rapp et al.,[21] the rate constant of reaction 1, k_1, is 6×10^{-13} cm^3/s. Hoell et al.[23] evaluated the validity of k_2/k_1 ratio with the presence of diluting gases such as N_2 and stated that $k_2/k_1 \approx 1$ was realistic to describe the generation and loss of F. Therefore, we assumed $k_1 = k_2 = 6 \times 10^{-13}$ cm^3/s in this study. Densities per unit volume of F_2, N_{F_2}, and NO, N_{NO}, were calculated by the ideal gas law.

$$N = n/V = P/RT \quad (3)$$

where P was the partial pressure of F_2 and NO (P_{F_2} = 14.8 Pa, P_{NO} = 0−44 Pa), V was the volume, R was the gas constant (R = 8.314 J/mol-K), and T was the temperature inside the chamber by assuming that the increase in the temperature due to the exothermic reaction of eq 1 was negligible (T = 300 K). On the basis of eq 3, the net density of F present in the unit volume, $N_{F\text{-net}}$, by reactions 1 and 2 was calculated. First, the density of F generated by the reaction 1, $N_{F\text{-generation}}$, was calculated by

$$dN_{F\text{-generation}}/dt = k_1 N_{F_2} N_{NO} \quad (4)$$

$$N_{F\text{-generation}} = k_1 N_{F_2} N_{NO} t = k_1 N_{F_2} N_{NO} \tau = 0 \sim 1.2 \times 10^{-2}\ mol/m^3 \quad (5)$$

where τ was the residence time of the process gas in the Pyrex tube (1.9×10^{-3} s), which was calculated by the volume of the tube, V (7.6×10^{-5} m^3), divided by the effective pumping speed at 3.9×10^{-2} m^3/s. The reminder of NO density after the reaction 1, N_{NO}', was calculated by subtracting $N_{F\text{-generation}}$ from N_{NO} ($(0-5.8) \times 10^{-3}$ mol/m^3). Because $N_{F\text{-generation}} > N_{NO}'$, reaction 2 was limited by the N_{NO}'. Therefore, the density of FNO, which was the same as the density loss of F, $N_{F\text{-loss}}$, could be calculated as

$$dN_{F\text{-loss}}/dt = k_2 N_F N_{NO}' = k_1 N_{NO}'^2 = k_1 (N_{NO} - N_{F\text{-generation}})^2 \quad (6)$$

dx.doi.org/10.1021/jp3119132 | J. Phys. Chem. C 2013, 117, 5118−5125

$$N_{\text{F-loss}} = k_1(N_{\text{NO}} - N_{\text{F-generation}})^2 t \quad (7)$$

The net density of F, $N_{\text{F-net}}$, which was the difference between $N_{\text{F-generation}}$ and $N_{\text{F-loss}}$, was calculated from eqs 5 and 7 by substituting $t = \tau$.

$$N_{\text{F-net}} = N_{\text{F-generation}} - N_{\text{F-loss}} = 0 \sim 8.1 \times 10^{-3}\ \text{mol/m}^3 \quad (8)$$

The flux of the F approaching the Si surface, Γ_{F}, was estimated as[35]

$$\Gamma_{\text{F-net}} = 1/4 \cdot N_{\text{F-net}} \cdot \bar{v}_{\text{F}} \quad (9)$$

where $\bar{v}_{\text{F}}$ was the average speed of F at 576 m/s at T = 300 K. According to Ninomiya et al.,[36] 10% of the $\Gamma_{\text{F-net}}$ approaching the Si surface reacted with Si to form a SiF_4 to complete the etching reaction. Therefore, the F flux responsible for etching, $\Gamma_{\text{F-react}}$, could be calculated by multiplying the reaction probability, γ_r, of 0.1.

$$\Gamma_{\text{F-react}} = \gamma_r \cdot \Gamma_{\text{F-net}} \quad (10)$$

Changes in the $\Gamma_{\text{F-react}}$ with respect to the $f_{\text{NO}}/f_{\text{F}_2}$ are depicted in Figure 6 with the dotted line. The $\Gamma_{\text{F-react}}$ increased with $f_{\text{NO}}/f_{\text{F}_2}$. The etch rate and the $\Gamma_{\text{F-react}}$ showed the similar trend up to the $f_{\text{NO}}/f_{\text{F}_2} \approx 1.0$ with respect to the change in the $f_{\text{NO}}/f_{\text{F}_2}$. This indicated that the increase in the etch rate in this region was based on the increase in supplied F from the gas phase. However, the etch rate and the $\Gamma_{\text{F-react}}$ showed the opposite trend at $1.0 < f_{\text{NO}}/f_{\text{F}_2} < 2.0$, where the etch rate was reduced to 20% at $1 < f_{\text{NO}}/f_{\text{F}_2} < 2$, whereas the $\Gamma_{\text{F-react}}$ increased ~25%. At the $f_{\text{NO}}/f_{\text{F}_2} > 2.3$, the etch rate decreased much more rapidly than that at $1.0 < f_{\text{NO}}/f_{\text{F}_2} < 2.0$, whereas the $\Gamma_{\text{F-react}}$ kept increasing with the $f_{\text{NO}}/f_{\text{F}_2}$.

4.4. Change in Surface Chemical Bonding Structure with the Addition of NO. To explain the discrepancy of the relationship between the etch rate and the $\Gamma_{\text{F-react}}$ with respect to the $f_{\text{NO}}/f_{\text{F}_2}$ at above 1.0, surface chemical bonding structures were measured by the transmission FT-IR, and the results are shown in Figure 7.

Five main peaks were observed in the wave numbers from 650 to 1350 cm^{-1}, that is, 643−767, 767−841, 865−1010, 1012−1137, and 1137−1311 cm^{-1}. Their peak height increased with the addition of NO. On the basis of the references and prediction of peak position of $Si_9H_{13}X$ (X = F_2, FNO, NO, F, OH, O_2) structures calculated by B3LYP/6-31G+(d,p) in Gaussian 09, the candidates of the chemical bonding structures are listed in Table 1. Absorbance spectra at 643−767 cm^{-1} correspond to the F−N═O asymmetric stretching (752 cm^{-1}). Absorbance spectra around 767−841 cm^{-1} correspond to the Si−O bending (810 cm^{-1}),[37] the Si−N stretching (820 cm^{-1}),[37] and the N−Si−F stretching (827 cm^{-1}). Absorbance spectra around 865−1010 cm^{-1} correspond to the Si−F stretching (940 cm^{-1}),[38] the Si-NO bending (900−1000 cm^{-1}), or both.[37] Absorbance spectra around 1012−1137 cm^{-1} correspond to the in-phase Si−O/Si═O stretching (1069,[38] 1075,[37] 1080,[40] and 1014 cm^{-1}[40] when the O is located in the backbone of the Si−Si and 1102 cm^{-1} when the Si═O bond formed at the surface). Absorbance spectra around 1137−1311 cm^{-1} correspond to the out-of-phase Si−O/Si═O stretching (1130−1150 cm^{-1})[39] and the Si−N═O stretching (1181 cm^{-1} when N═O was placed in the middle of the Si−Si backbone).

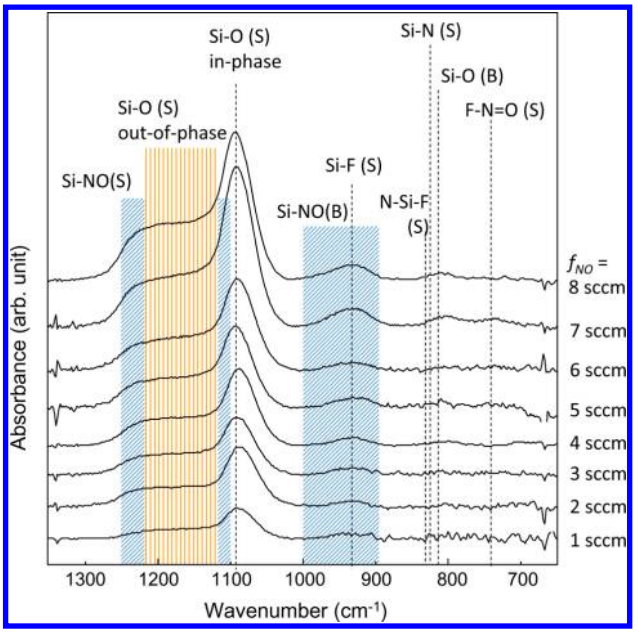

Figure 7. FT-IR absorbance spectra obtained from the nondoped Si sample etched in the mixture of f_{NO} = 1−8 sccm, f_{Ar} = 46.5−53.5 sccm, and $f_{\text{Ar/5\%-F2}}$ = 54.5 sccm, corresponding f_{F_2} = 2.7 sccm while maintaining the chamber pressure at 600 Pa during the process time of 0.5 min.

FT-IR results confirmed the presence of the −F, ═O/−O, −NO, and −FNO functional groups at the surface of Si, as shown in Figure 4 and 5. The presence of ═O/−O peaks was due to the post-etching reaction between the dangling bond at the Si surface and O_2 in the atmosphere. The broad absorbance spectra at 1137−1311 cm^{-1} were the indication of the presence of the Si−NO/Si−FNO bonds with different chemical bonding structures, as shown in Figure 5. The significant increase in peak intensities at 865−1010, 1012−1137, and 1137−1311 cm^{-1} was observed with the increase in the $f_{\text{NO}}/f_{\text{F}_2}$, indicating the presence of the dangling bond that can react O_2 in the air and Si−NO at the Si surface with the addition of NO.

4.5. Change in Etched Morphology with the Addition of NO. The side and the bottom walls of the etched Si samples at different $f_{\text{NO}}/f_{\text{F}_2}$ were observed by SEM, and representative results are shown in Figure 8. Unlike conventional plasma-induced Si etching,[35] it was found that etched surface became rough with the addition of NO to F_2, as shown in Figure 8a. The etched Si bottom and the side surfaces treated at $f_{\text{NO}}/f_{\text{F}_2} \sim 1.5$ (Figure 8a, f_{NO} = 4 sccm) had three different sizes of surface pits whose diameters were (i) 50−100 nm, (ii) 300−600 nm, and (iii) 2−5 μm, as shown in Figure 8b. The top view of the etched bottom surface is shown in Figure 8c at f_{NO} = 1, 3, and 8 sccm. The change in the density of three different sizes of etch pits (i)~(iii) was observed with the addition of NO. Etch pits (i) and (iii) were first initiated at the f_{NO} = 1 sccm ($f_{\text{NO}}/f_{\text{F}_2} \sim 0.4$), followed by the increase in etch pits (ii) at the f_{NO} = 3 sccm ($f_{\text{NO}}/f_{\text{F}_2} \sim 1.1$). The etch rate was maximum under this condition, as shown in Figure 6. When the f_{NO} = 8 sccm ($f_{\text{NO}}/f_{\text{F}_2} \sim 2.9$) was added to F_2, etch pits (i) and mesh-like structures were observed, but the etch pits (ii) and (iii) were not observed.

Surface morphology of nondoped Si (100) etched for 30 s was measured by SWLI, and results are shown in Figure 9. The

dx.doi.org/10.1021/jp3119132 | J. Phys. Chem. C 2013, 117, 5118−5125

Table 1. Candidate of the Chemical Bonding Structure of the Observed FT-IR Peaks from the Si Surface Etched in NO/F_2 Gas Mixture at Room Temperature in Figure 7

peak no.	wave numbers	candidate of the chemical bonding structure
1	643−767 cm^{-1}	F−N═O asymmetric stretching (752 cm^{-1})
2	767−841 cm^{-1}	Si−O bending (810 cm^{-1})[37]
		Si−N stretching (820 cm^{-1})[37]
		N−Si−F stretching (827 cm^{-1})
3	865−1010 cm^{-1}	Si−F stretching (940 cm^{-1})[38]
		Si−NO bending (900−1000 cm^{-1})[37]
4	1012−1137 cm^{-1}	in-phase Si−O/Si═O stretching (1069 cm^{-1},[38] 1075 cm^{-1},[37] 1080 cm^{-1},[40] and 1014 cm^{-1}[40] when the O is located in the backbone of the Si−Si, 1102 cm^{-1} when the Si═O bond formed at the surface)
5	1137−1311 cm^{-1}	out-of-phase Si−O/Si═O stretching (1130−1150 cm^{-1}),[39] Si−N═O stretching (1181 cm^{-1} when N═O was placed in the middle of the Si−Si backbone)

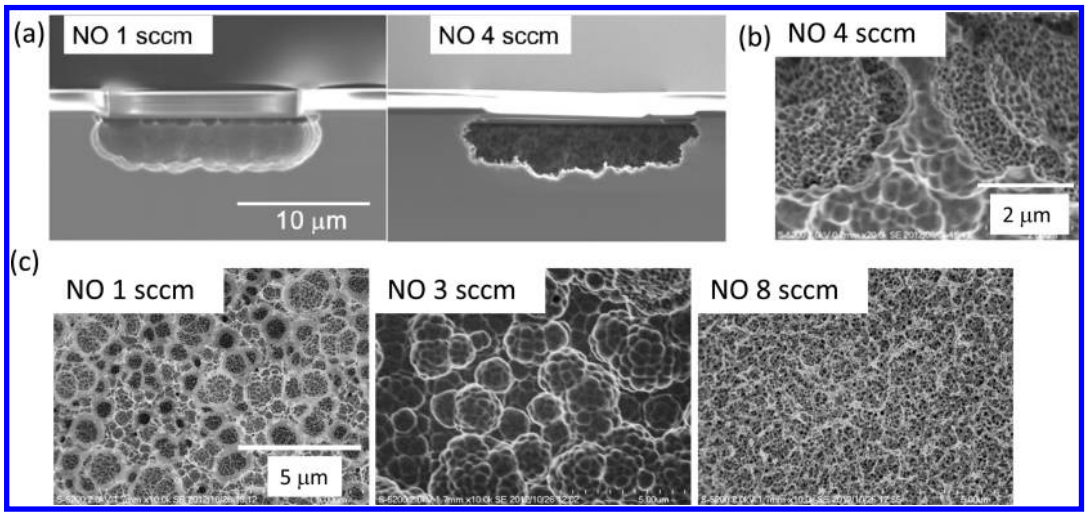

Figure 8. SEM images of the etched feature of the p-type Si (100) samples after exposing to the NO/F_2 gas mixture for 5 min. Patterned Si wafer was etched while changing the NO flow rate f_{NO} = 1−8 sccm and the Ar flow rate f_{Ar} = 46.5−53.5 sccm with the constant $f_{Ar/5\%\text{-}F2}$ at 54.5 sccm, corresponding f_{F_2} at 2.7 sccm, and the chamber pressure at 600 Pa. (a) Cross-sectional images of the etched feature with the SiO_2 mask consisting of 15 μm × 15 μm square opening. (b) High-resolution SEM image of the bottom surface of the etched feature. (c) Top view of the etched bottom surface exposed in the gas mixture.

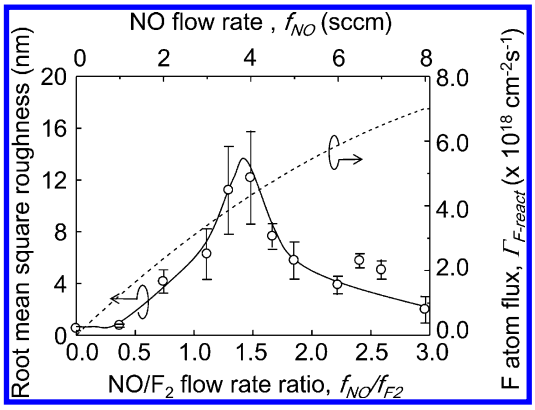

Figure 9. Relationship between the surface roughness and the flow rate ratio, f_{NO}/f_{F_2}. $f_{Ar\text{-}5\%F2}$ = 54.5 sccm (corresponding f_{F_2} = 2.7 sccm) remained constant while varying f_{NO} from 0.0 to 8.0 sccm and f_{Ar} from 46.5 to 54.5 sccm. The pressure of the chamber was maintained at 600 Pa throughout the process time of 0.5 min. 10% of F atom flux approaching the Si surface, the $\Gamma_{F\text{-react}}$, was calculated and shown by the dotted line.

$\Gamma_{F\text{-react}}$ determined in Section 4.3 was also plotted with the dotted line in Figure 9. Rms roughness increased proportionally to the squares of the f_{NO}/f_{F_2} up to f_{NO}/f_{F_2} = 1.25 to 1.5 and decreased rapidly above f_{NO}/f_{F_2} = 1.5. The maximum rms roughness of Si etched at f_{NO}/f_{F_2} = 1.25 to 1.5 was 12 times higher than that of Si treated at f_{NO}/f_{F_2} = 0. Rms roughness at f_{NO}/f_{F_2} = 3.0 became less than 1/6 of that at f_{NO}/f_{F_2} = 1.25 to 1.5. The rms roughness, the etch rate, and the F atom flux did not have correlation by comparing Figures 6 and 9. The change in the rms roughness with the different f_{NO}/f_{F_2} can be explained by the presence of the Si_xH_y-F_2, Si_xH_y-NO, Si_xH_y-F, and Si_xH_y-FNO chemical bonding structures shown in Figures 3, 4, 5, and 7 based on the MO calculations and FT-IR measurement results. The etch rate reduction between 1.0 < f_{NO}/f_{F_2} < 2.0 could be explained by the presence of Si−NO and Si−NO−Si−F bonds at the surface that would partially interfere with the F and F_2 reaction to Si. Furthermore, when f_{NO}/f_{F_2} > 1.5, a significant amount of Si−NO or the Si−NO−Si−F bonds was formed at the Si surface that would completely block the dangling bond at the Si surface for the reaction between Si and F or F_2. This would lead the drastic etch rate

dx.doi.org/10.1021/jp3119132 | J. Phys. Chem. C 2013, 117, 5118−5125

and roughness reduction shown in Figures 6 and 9 at $f_{NO}/f_F > 1.5$.

The formation of different chemical bonding structures of Si_xH_y-F_2, Si_xH_y-NO, Si_xH_y-F, and Si_xH_y-FNO at the Si surface that was calculated and measured in this study is considered to be the main cause of forming textured surface with different sizes of micro- and nanoscale etch pits, as shown in Figures 8 and 9. The model surface of H-terminated Si that reacted with F_2, NO, F, and FNO is depicted in Figure 10a. Different sizes of

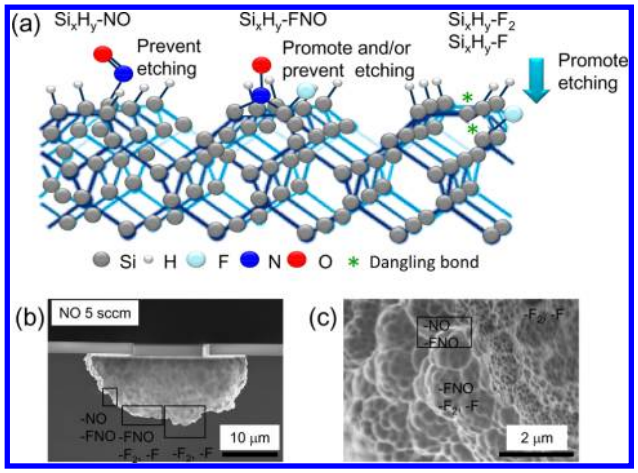

Figure 10. (a) Model Si surface with the presence of F_2, NO, F, and FNO. (b) Cross-sectional SEM image of the etched feature of Si with the presence of different sizes of etch pits. (c) Magnified view of the etch pits of panel b. The SEM images of panels b and c were taken from the cross-section of the Si with the SiO_2 mask consisting of the 8 μm × 8 μm square opening when the sample was exposed to f_{NO} = 5 sccm and the Ar flow rate f_{Ar} = 49.5 sccm while maintaining the constant $f_{Ar/5\%\text{-}F2}$ at 54.5 sccm, corresponding f_{F_2} at 2.7 sccm, and the chamber pressure at 600 Pa.

etch pits shown in Figure 8 are considered to be initiated by the different Si etch rate by the presence of chemisorbed F_2, NO, F, and FNO at the Si surface, the location of the dangling bonds formed by the reaction of F_2, NO, F, and FNO with Si, and the generation of desorbed molecules such as SiF_2 and SiF_4.

When F_2 reacts with Si with the dangling bond, modeled as Si_9H_{13} in this study, the new dangling bond is formed and the first and the second layers of Si−Si bonds are broken, as shown in Figure 4. The formation of this new dangling bond at the Si surface may react with another F_2, NO, F, and FNO, leading to initiate a new dangling bond or to form SiF, SiF_2, SiF_3, and SiF_4. The removal of Si atoms from the different layers of Si lattice by desorbing SiF_2 or SiF_4 molecules leaves etch pits with various sizes. The same phenomena − the cascade of the dangling bond formation, dangling bond reaction to F_2 and F, formation and desorption of SiF_2 and SiF_4, and the creation of etch pits − may be observed when Si with the dangling bond reacts with FNO. One or two new dangling bonds may be initiated when FNO reacts with Si by breaking Si−Si bonds as shown in Figure 5b, reaction steps n = 39 and 46. FNO may also form a chemical bonding structure of Si_xH_y-FNO without the initiation of the new dangling bond, as shown in Figure 5b, reaction steps n = 13 and 48. When these chemical bonding structures are present at the Si surface, the etching would be prevented to form island, as shown in Figures 10b and 10c.

F may react with the dangling bond at the Si surface without initiating the new dangling bond, as shown in Figure 4c, but F may react with the H-terminated Si without the dangling bond to form a new dangling bond by extracting HF, as shown in Figure 3. Therefore, the same reaction cascade to form etch pits by the reaction of F_2 or FNO with Si is expected with the chemical reaction between F and Si_xH_y. On the contrary, NO reacts with the dangling bond at the Si surface without forming a new dangling bond, inhibiting the further chemical reaction of Si with F_2, F, and FNO. Therefore, the surface would not be etched, and the island formation would be expected, as shown in Figures 10b and 10c. All gas-phase molecules and atoms such as F_2, NO, F, and FNO react with Si at different speeds. The reaction site and the position of the newly formed dangling bonds that would initiate the etching and the speed of the formation of desorbing molecules such as SiF_2 and SiF_4 are random. From these reasons, unique surface morphology with different sizes of etch pits (i)∼(iii) shown in Figure 8 is formed by the chemical dry etching using NO/F_2 at room temperature.

We have evaluated the use of NO/F_2 gases at room temperature to texture the surface of the single-crystal Si solar panel to improve the efficiency of converting light into electricity by reducing reflectance from the Si surface. Preliminary results showed that the reflectance of nondoped Si surface etched in the NO/F_2 gas mixture at $f_{NO}/f_{F_2} \approx 1.0$ to 2.0 was ∼20%, which was 1/2 of the reflectance of untreated Si. These results indicate that the Si surface texturing using the NO/F_2 gas mixture is the effective method to promote the light absorbance of solar cells by reducing the reflectance significantly.

5. CONCLUSIONS

The NO/F_2 gas mixture was successfully used for the plasmaless Si etching using the reaction of F_2 + NO → FNO + F. According to the MO calculation, F at the excess energy of 0.8 eV was generated by mixing NO and F_2 at a room temperature. We found that F must be present to start the etching process at the Si−H-terminated surface by calculating the changes in chemical bonding structures and total energies before and after the reaction of F_2, NO, F, and FNO with Si_9H_{14} by the MO method using the Si(100)-2×1 cluster model. Once the dangling bond was generated by the reaction of Si_9H_{14} + F → Si_9H_{13} + HF, F_2, NO, F, and FNO may exothermically react with Si_9H_{13}. NO and F reacted at the dangling bond to form the Si−NO and the Si−F bonds, whereas F_2 and FNO broke the Si−Si bond and formed the Si−F and the Si−NO−Si−F bonds.

Si etch rates, surface chemical bonding structures, and surface morphology were measured when Si was exposed to NO/F_2 mixtures at a room temperature while changing the f_{NO}/f_{F_2}. F flux was calculated based on the generation of F (F_2 + NO → FNO + F) and the loss of F (F + NO → FNO). The etch rate and rms roughness increased up to the f_{NO}/f_{F_2} = 1.0 due to the increase in the F flux from the gas phase. However, the Si etch rate gradually decreased at $1.0 < f_{NO}/f_{F_2} < 2.0$ by the formation of the Si−NO or the Si−NO−Si−F bonds that would partially block the Si etching by F and F_2, forming nonuniform etch pits, even though F flux was increased. Further addition of NO formed the dense Si−NO or Si−NO−Si−F bonds at the Si surface that would completely block dangling bonds for F and F_2 reaction, producing the smooth surface.

dx.doi.org/10.1021/jp3119132 | J. Phys. Chem. C 2013, 117, 5118−5125

AUTHOR INFORMATION

Corresponding Author

*Tel/Fax: +81-52-788-6077. E-mail: stajima@plasma.engg.nagoya-u.ac.jp.

Notes

The authors declare no competing financial interest.

ACKNOWLEDGMENTS

We greatly acknowledge the research support funding provided by Tatematsu Zaidan, Aichi, Japan.

REFERENCES

(1) Saito, Y. *Sens. Mater.* **2002**, *14*, 231−237.
(2) Savastiouk, S.; Siniaguine, O.; Diorio, M. *Adv. Packag.* **1998**, *7*, 55−58.
(3) Arana, L. R.; de Mas, N.; Schmidt, R.; Franz, A. J.; Schmidt, M. A.; Jensen, K. F. *J. Micromech. Microeng.* **2007**, *17*, 384−392.
(4) Pruette, L. C.; Karecki, S. M.; Reif, R.; Langan, J. G.; Rogers, S. A.; Ciotti, R. J.; Felker, B. S. *J. Vac. Sci. Technol., A* **1998**, *16*, 1577−1581.
(5) Williams, K. R.; Muller, R. S. *J. Microelectromech. Syst.* **1996**, *5*, 256−269.
(6) Reinhardt, K. A.; Kern, W. *Handbook of Silicon Wafer Cleaning Technology*, 2nd ed.; Materials Science and Process Technology Series; William Andrew: Norwich, NY, 2007; Chapter 1.
(7) Ibbotson, D. E.; Mucha, J. A.; Flamm, D. L.; Cook, J. M. *J. Appl. Phys.* **1984**, *56*, 2939−2942.
(8) Ibbotson, D. E.; Flamm, D. L.; Mucha, J. A.; Donnelly, V. M. *Appl. Phys. Lett.* **1984**, *44*, 1129−1131.
(9) Seki, T.; Yoshino, T.; Senoo, T.; Koike, K.; Nomnimiya, S.; Aoki, T.; Matsuo, J. *AIP Conf. Proc.* **2010**, *1321*, 317−320.
(10) Flamm, D. L.; Herb, G. K. *Plasma Etching: An Introduction*; Manos, D. M., Flamm, D. L., Eds.; Academic: New York, 1989.
(11) Hwang, G. S.; Anderson, C. M.; Gordon, M. J.; Moore, T. A.; Minton, T. K.; Giapis, K. P. *Phys. Rev. Lett.* **1996**, *77*, 3049−3052.
(12) Giapis, K. P.; Moore, T. A.; Minton, T. K. *J. Vac. Sci. Technol., A* **1995**, *13*, 959−965.
(13) Gray, D. C.; Tepermeister, I.; Sawin, H. H. *J. Vac. Sci. Technol., B* **1993**, *11*, 1243−1257.
(14) Weakliem, P. C.; Carter, E. A. *J. Chem. Phys.* **1993**, *98*, 737−745.
(15) Jakob, P.; Chabel, Y. J.; Raghavachari, K.; Becker, R. S.; Becker, A. *J. Surf. Sci.* **1992**, *275*, 407−413.
(16) Weakliem, P. C.; Wu, C. J.; Carter, E. A. *Phys. Rev. Lett.* **1992**, *69*, 200−203.
(17) Schoolcraft, T. A.; Garrison, B. J. *J. Am. Chem. Soc.* **1991**, *113*, 8221−8228.
(18) Flamm, D. L.; Donnelly, V. M.; Mucha, J. A. *J. Appl. Phys.* **1981**, *52*, 3633−3639.
(19) Martin, M.; Cunge, G. *J. Vac. Sci. Technol., B* **2008**, *26*, 1281−1288.
(20) Gottscho, R. A.; Jurgensen, C. W.; Vitkavage, D. J. *J. Vac. Sci. Technol., B* **1992**, *10*, 2133−2147.
(21) Rapp, D.; Johnston, H. S. *J. Chem. Phys.* **1960**, *33*, 695−699.
(22) Cool, T. A.; Shirley, J. A.; Stephens, R. R. *Appl. Phys. Lett.* **1970**, *17*, 278.
(23) Hoell, J. M., Jr.; Allario, F.; Jarrett, O., Jr.; Seals, R. K., Jr. *J. Chem. Phys.* **1973**, *58*, 2896−2901.
(24) Kolb, C. E. *J. Chem. Phys.* **1976**, *64*, 3087−3090.
(25) Jones, W. E.; Skolnik, E. G. *Chem. Rev.* **1976**, *76*, 563−592.
(26) Yun, Y. B.; Park, S. M.; Kim, D. J.; Lee, N. -E.; Choi, C. K.; Kim, K. S.; Bae, G. H. *Thin Solid Films* **2008**, *516*, 3549−3553.
(27) Yun, Y. B.; Park, S. M.; Lee, N.-E. *J. Korean Phys. Soc.* **2008**, *53*, 2386−2390.
(28) Yun, Y. B.; Park, S. M.; Kim, D. J.; Lee, N. -E.; Kim, K. S.; Bae, G. H. *J. Vac. Sci. Technol., A* **2007**, *25*, 980−985.
(29) Heo, W.; Ahn, J. H.; Lee, N.-E. *J. Vac. Sci. Technol., A* **2010**, *28*, 1073−1077.
(30) Park, A. M.; Ahn, J. H.; Kim, S. I.; Lee, N.-E. *J. Korean Phys. Soc.* **2009**, *54*, 1127−1130.
(31) Shigemoto, T.; Sonobe, J. *ECS Trans.* **2007**, *11*, 47−54.
(32) Kameda, K.; Sonobe, J.; Tadaki, Y. Japanese Patent JP P2011-233570A, 2011.
(33) Tamaoki, N.; Sato, Y.; Seta, S.; Regis, J.; Sonobe, J. ; Kimura, T. ; Momota, K. Japanese Patent JP 4739709 B2, 2011.
(34) Detailed description of Gaussian program is listed in http://www.gaussian.com/; accessed Jan 9, 2013.
(35) Lieberman, M. A.; Lichtenberg, A. J. *Principles of Plasma Discharges and Materials Processing*, 2nd ed.; John Wiley & Sons, Inc.: Hoboken, NJ, 2005; Chapter 15.
(36) Ninomiya, K.; Suzuki, K.; Nishimatsu, S.; Okada, O. *J. Appl. Phys.* **1985**, *58*, 1177−1182.
(37) Diniz, J. A.; Tatsch, P. J.; Pudenzi, M. A. A. *Appl. Phys. Lett.* **1996**, *69*, 2214−2215.
(38) Kim, Y.-H.; Hwang, M. S.; Kim, H. J.; Kim, J. Y.; Lee, Y. *J. Appl. Phys.* **2001**, *90*, 3367−3370.
(39) San Andrés, E.; del Prado, A.; Martínez, F. L.; Mártil, I.; Bravo, D.; Lopxez, F. J. *J. Appl. Phys.* **2000**, *87*, 1187−1192.
(40) Pandey, R. K.; Patil, L. S.; Bange, J. P.; Patil, D. R.; Mahajan, A. M.; Patil, D. S.; Gautam, D. K. *Opt. Mater.* **2004**, *25*, 1−7.